Druitt, T.H., Kutterolf, S., Ronge, T.A., and the Expedition 398 Scientists
Proceedings of the International Ocean Discovery Program Volume 398
publications.iodp.org

Site U1594[1]

Keywords
International Ocean Discovery Program, IODP, R/V *JOIDES Resolution*, Expedition 398, Hellenic Arc Volcanic Field, Earth Connections, Earth in Motion, Biosphere Frontiers, Site U1594, Santorini caldera, Aegean Sea, Christiana-Santorini-Kolumbo volcanic field, subduction zone, shallow-marine volcanism

Core descriptions

Supplementary material

References (RIS)

MS 398-108
Published 30 July 2024

Funded by NSF OCE1326927, ECORD, and JAMSTEC

S. Kutterolf, T.H. Druitt, T.A. Ronge, S. Beethe, A. Bernard, C. Berthod, H. Chen, S. Chiyonobu, A. Clark, S. DeBari, T.I. Fernandez Perez, R. Gertisser, C. Hübscher, R.M. Johnston, C. Jones, K.B. Joshi, G. Kletetschka, O. Koukousioura, X. Li, M. Manga, M. McCanta, I. McIntosh, A. Morris, P. Nomikou, K. Pank, A. Peccia, P.N. Polymenakou, J. Preine, M. Tominaga, A. Woodhouse, and Y. Yamamoto[2]

[1] Kutterolf, S., Druitt, T.H., Ronge, T.A., Beethe, S., Bernard, A., Berthod, C., Chen, H., Chiyonobu, S., Clark, A., DeBari, S., Fernandez Perez, T.I., Gertisser, R., Hübscher, C., Johnston, R.M., Jones, C., Joshi, K.B., Kletetschka, G., Koukousioura, O., Li, X., Manga, M., McCanta, M., McIntosh, I., Morris, A., Nomikou, P., Pank, K., Peccia, A., Polymenakou, P.N., Preine, J., Tominaga, M., Woodhouse, A., and Yamamoto, Y., 2024. Site U1594. In Druitt, T.H., Kutterolf, S., Ronge, T.A., and the Expedition 398 Scientists, Hellenic Arc Volcanic Field. Proceedings of the International Ocean Discovery Program, 398: College Station, TX (International Ocean Discovery Program). https://doi.org/10.14379/iodp.proc.398.108.2024
[2] **Expedition 398 Scientists' affiliations.**

1. Background and objectives

Site U1594 (proposed Site CSK-07B) is located in the southern basin of Santorini caldera at a water depth of 291 meters below sea level (mbsl) (Figure **F1**). It was drilled to a maximum recovery depth of 50.1 meters below seafloor (mbsf) in a single hole (U1594A) with 93% recovery before hole instability set in and the hole was terminated (all depths below seafloor are given using the core depth below seafloor, Method A [CSF-A] scale, except in **Operations** where the drilling depth below seafloor [DSF] scale is used). Site U1595 addresses the same drilling objectives and lies southwest of Site U1594. Two additional sites (U1596 and U1597) lie in the northern caldera basin.

Four seismic units have been recognized in the caldera (Johnston et al., 2015; Nomikou et al., 2016) (Figure **F2**). They were thought to consist of muds and sands from cliff mass wasting (Seismic Unit S1); compacted (possibly lithified) sandy volcaniclastics from Kameni Volcano (Unit S2);

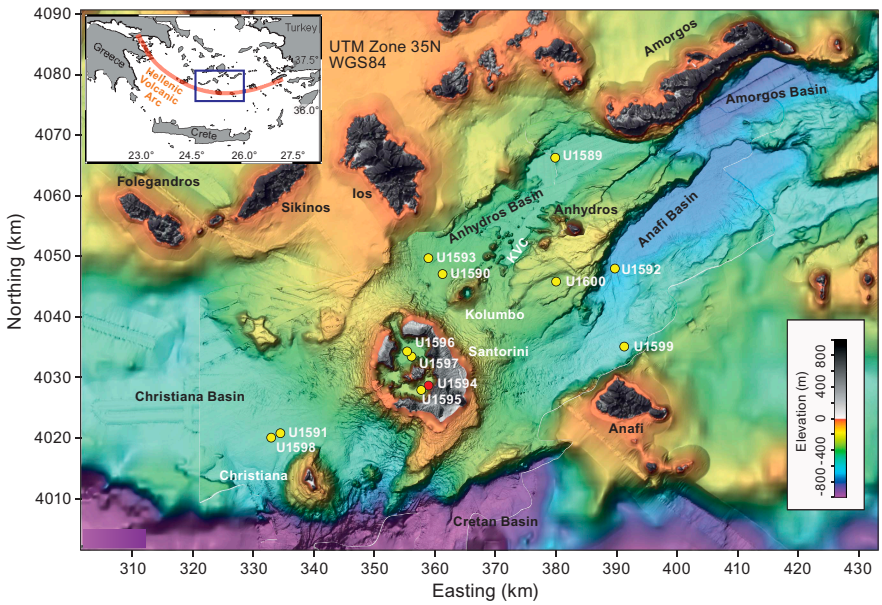

Figure F1. Site map. Red = Site U1594, yellow = other sites. Inset: location map. See Figure F1 in the Site U1589 chapter (Druitt et al., 2024) for citations for the swath data on which this map is based. KVC = Kolumbo volcanic chain.

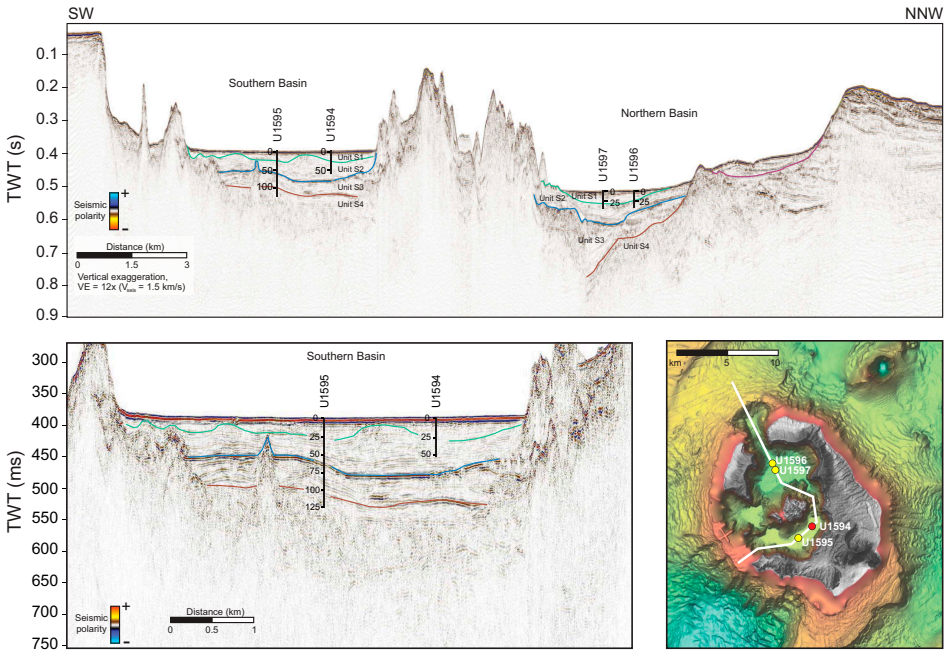

Figure F2. Top: seismic profile across the Santorini caldera with Seismic Units S1–S4, Sites U1594–U1597. Depths in meters. TWT = two-way traveltime. Bottom left: profile of Sites U1594 and U1595. Right: locations of the four intracaldera sites. Red = Site U1594, yellow = other sites.

and consolidated coarse blocky intracaldera tuffs, landslide debris, and/or flood gravels (Unit S3). Unit S4 was thought to be intracaldera tuff from the Late Bronze Age eruption. The four caldera sites were planned to sample Units S1–S3; test the published correlations between the two caldera basins; penetrate below Unit S3 into Unit S4; and address scientific Objectives 1, 4, 5, and 7 of the Expedition 398 Scientific Prospectus (Druitt et al., 2022). By drilling both caldera basins and exploiting our dense seismic reflection coverage, we gained access to the 3D architecture of the entire caldera fill. We also targeted the question of why the northern basin is 100 m deeper than the southern one. Finally, we tested whether Unit S3 consisted of flood debris from the caldera flooding event (Nomikou et al., 2016) or was Late Bronze Age intracaldera tuff (Johnston et al., 2015). The intracaldera sites were used for microbiological work of scientific Objective 7.

2. Operations

On 22 January 2023 at 1830 h, the vessel arrived at Site U1594 at the southern end of the Santorini caldera. All thrusters were down and secured at 1848 h. The vessel was switched to dynamic positioning control, and Site U1594 was started at 1850 h (all times local; 2 h ahead of UTC). The 15.0 nmi transit took 1.8 h at an average speed of 8.3 kt.

2.1. Hole U1594A

Once given the all clear, the rig crew made up an advanced piston corer/extended core barrel (APC/XCB) bottom hole assembly (BHA) with a bit. Hole U1594A (36°23.3368′N, 25°25.0290′E) was spudded on 22 January 2023 at 2310 h. The core was shot from 297.0 meters below rig floor, with a recovery of 4.2 m, establishing the seafloor at 291.0 mbsl (Table **T1**).

APC coring continued on 23 January with Cores 2H (4.2 mbsf) through 6H, with the bottom at 51.7 mbsf, the final depth for Hole U1594A. Excessive torque was observed, indicating a collapsing hole. The driller worked the drill string, but the tight conditions persisted. The drill string was pulled up with the top drive from 42.2 mbsf to ~100 m above seafloor. The bit cleared the seafloor at 0350 h.

Table T1. Core summary, Site U1594. mbsf = meters below seafloor. NA = not applicable. DSF = drilling depth below seafloor. H = APC. **Download table in CSV format.**

Hole U1594A
Latitude: 36°23.3368′N
Longitude: 25°25.0290′E
Water depth (m): 291
Date started (UTC): 1645 h; 22 January 2023
Date finished (UTC): 0245 h; 23 January 2023
Time on hole (days): 0.42
Penetration (mbsf): 51.7
Cored interval (m): 51.7
Recovered length (m): 47.94
Recovery (%): 92.73
Drilled interval (m): N/A
Drilled interval (no.): 0
Total cores (no.): 6
APC cores (no.): 6

Core	Top depth drilled DSF (m)	Bottom depth drilled DSF (m)	Interval advanced (m)	Recovered length (m)	Core recovery (%)	Core on deck date (2023)	Core on deck time UTC (h)
398-U1594A-							
1H	0.0	4.2	4.2	4.22	100	22 Jan	2120
2H	4.2	13.7	9.5	9.51	100	22 Jan	2215
3H	13.7	23.2	9.5	9.21	97	22 Jan	2245
4H	23.2	32.7	9.5	8.42	89	22 Jan	2320
5H	32.7	42.2	9.5	8.69	91	22 Jan	2350
6H	42.2	51.7	9.5	7.89	83	23 Jan	0030
		Totals:	51.7	47.94			

The decision was made to move the vessel to an alternate offset site in the southern caldera (Site U1595). The vessel was moved in dynamic positioning mode, starting the 0.7 nmi passage at 0445 h and marking the end of Site U1594.

3. Lithostratigraphy

Cores from Site U1594 recovered a coherent stratigraphy from 0 to 50.09 mbsf (Sections 398-U1594A-1H-1 through 6H-6) (Figure **F3**). The site consists only of Hole U1594A.

The recovered material is unlithified sediment dominated by volcanic material with minor amounts of mud and tuffaceous mud in the uppermost 1.5 m. Smear slides for microscopic analyses were prepared to confirm macroscopic descriptions of distinct lithology changes at the section level, such as identification of vitric ash particles in tuffaceous lithologies or crystals in ash layers. X-ray diffraction (XRD) data were obtained from three interstitial water (IW) squeeze cake sediment residues from Hole U1594A.

Figure **F3** summarizes the lithostratigraphy of Site U1594, displaying core recovery and lithostratigraphic unit and subunits. Table **T2** provides the upper and lower boundaries and thicknesses and lithologic summaries of the unit and subunits. Figure **F4** graphically presents the relative proportions of volcanic, tuffaceous, and nonvolcanic lithologies in Hole U1594A, and Figure **F5** presents the grain size distribution of the sediments, in particular the changes in grain size in the volcanic-dominated unit, to graphically show the distribution of ash, lapilli-ash, and lapilli. Figure **F6** displays different types of core disturbance observed at Site U1594.

The following sections describe (1) the effects of core disturbance, (2) the lithostratigraphic unit and subunits, and (3) XRD results from Site U1594.

3.1. Core disturbance

The following types of core disturbance disrupt the lithostratigraphy at Site U1594 (Figure **F6**):

- Fall-in: coarse clast-supported or, in some cases, finer grained muddy intervals at the tops of many cores (Figure **F6A**). In these intervals, which may reach up to 16 cm in thickness, original lithofacies and sedimentary structures are usually slightly disturbed and not fully destroyed.
- Soupy: typically restricted to water-saturated intervals of unconsolidated ash overprinting original sedimentary or depositional structures (Figure **F6B**).
- Artificial size and density segregation: likely to occur during drilling or with postrecovery core handling processes on board (e.g., inclining, shaking, and plunging cores on the catwalk to compact sediments). Jutzeler et al. (2014) also described pseudohorizontal density grading that can occur while the core is lying flat on deck, resulting in vertical structures once the core is

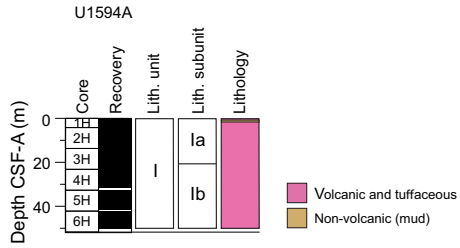

Figure F3. Lithostratigraphic summary, Site U1594. Unit color = dominant lithology.

Table T2. Lithostratigraphic unit and subunits, Hole U1594A. * = bottom not recovered, end of hole. **Download table in CSV format.**

Lith. unit	Subunit	Top depth (mbsf)	Top core, section, interval (cm)	Bottom depth (mbsf)	Bottom core, section, interval (cm)	Thickness (m)	Lithologic summary
			398-U1594A-		398-U1594A-		
I	Ia	0.00	1H-1, 0	20.74	3H-5, 100	20.74	Volcanic-dominated succession of ash, lapilli-ash, and lapilli with a minor amount of mud in the upper section
	Ib	20.74	3H-5, 100	50.09*	6H-6, 89	>33.37	Volcanic-dominated succession of lapilli-ash and lapilli with lesser ash; mafic enclaves common in lapilli

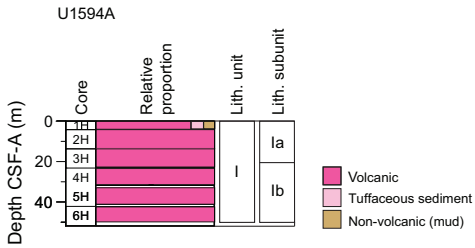

Figure F4. Relative percentages of volcanic, tuffaceous, and nonvolcanic lithologies, Hole U1594A. Unit I is volcanic dominated.

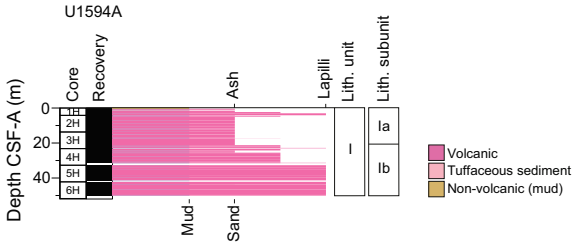

Figure F5. Grain size distribution of volcanic, tuffaceous, and nonvolcanic sediments, Site U1594. Length of colored bars = relative grain size (ash = <2 mm; lapilli = 2–64 mm; mud = <63 µm; sand = 0.063–2 mm), with separate scales shown for volcanic grain size (top) and nonvolcanic grain size (bottom; used for tuffaceous and nonvolcanic sediments). Mixed lithologies such as lapilli-ash (dark pink) that have relative grain sizes between two categories are plotted between ticks.

turned upright. Such core disturbance is observed most often in volcanic sediments because increased porosity allows sucking in of seawater during hydraulic piston coring. The resulting soupy texture allows material to flow within the core liner. Secondary normal or reverse grading, or density separation of clasts, may occur as a result of this disturbance and obscure primary sedimentary features.

3.2. Description of unit and subunits

3.2.1. Unit I

Interval: 398-U1594A-1H-1, 0 cm, to 6H-6, 89 cm (bottom of the hole)
Depth: 0.00–50.09 mbsf
Thickness: >50.09 m
Age: Holocene
Lithology: volcanic lithologies (ash, lapilli-ash, and lapilli), minor tuffaceous sediment (tuffaceous mud), and nonvolcanic sediment (mud)

Unit I is the only lithostratigraphic unit in Hole U1594A, extending from 0 to 50.09 mbsf (Table **T2**). It consists predominantly of volcanic lithologies (>75% volcanic particles; glass shards, pumice, scoria, and crystals) with small amounts of tuffaceous sediment (25%–75% volcanic particles) and nonvolcanic sediment (<25% volcanic particles) (Figure **F4**).

Volcanic lithologies comprise ash, lapilli-ash, and lapilli. Description of these lithologies in volcanic intervals was based on the relative abundance of ash-sized (<2 mm) and lapilli-sized (2–64 mm) particles, as described in **Lithostratigraphy** in the Expedition 398 methods chapter (Kutterolf et al., 2024). Ash and lapilli were used when the proportion of one grain size was >75%, and lapilli-ash was used when both grain sizes were present but at <75% abundance (Fisher and Schmincke, 1984). Tuffaceous sediments comprise tuffaceous mud, whereas nonvolcanic sediments are muds that may be organic rich.

Subunits in Unit I were defined primarily by a distinct change of the volcanic lithologies and grain size and a distinct change in physical properties (see **Physical properties**), including moisture and density (MAD), *P*-wave velocities, magnetic susceptibility (MS), and natural gamma radiation (NGR), as follows:

- Subunit Ia (Sections 398-U1594A-1H-1, 0 cm, through 3H-5, 100 cm; 0–20.74 mbsf): ash-dominated succession of volcanic lithologies with a minor amount of mud.
- Subunit Ib (Sections 3H-5, 100 cm, through 6H-6, 89 cm; 20.74–50.09 mbsf): lapilli-ash and lapilli-dominated succession with lesser ash.

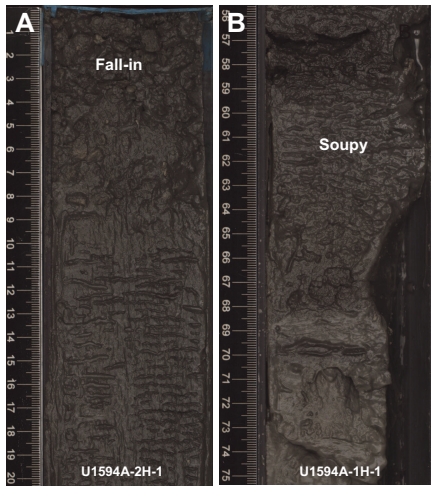

Figure F6. Core disturbances, Site U1594. A. Fall-in. B. Soupy.

3.2.1.1. Subunit Ia

Subunit Ia extends from 0 to 20.74 mbsf in Hole U1594A between Sections 1H-1, 0 cm, and 3H-5, 100 cm (Figure **F3**). It consists predominantly of volcanic lithologies (ash, lapilli-ash, and lapilli) with minor amounts of tuffaceous sediment (tuffaceous mud) and nonvolcanic sediment (mud) in the uppermost part of the succession (Figure **F7A, F7B**). Subunit Ia starts with 51 cm of brown organic-rich mud and gray mud with an intercalated 12 cm thick gray ash layer. This is followed by intervals of volcanic lithologies of ash, lapilli-ash, and lapilli, the majority of which are dominated by well-sorted olive-gray to very dark gray ash. Coarser grained volcanic intervals comprise moderately to poorly sorted grayish brown to very dark gray lapilli-ash and lapilli, with maximum grain sizes of medium to coarse lapilli. Pumice clasts are typically subangular with white, tan, dark brown, and dark gray varieties, often with lighter colored surfaces. Scoria clasts were described in two intervals of Subunit Ia. An interval of tuffaceous mud occurs at the lowermost part of Section 1H-1. The uppermost ash layers in this subunit are well sorted and very dark gray ash. Below this, intervals of ash are typically grayish brown in color, characterized by grain sizes ranging from fine to coarse ash, and moderately to poorly sorted. Minor amounts of dispersed light-colored subangular and medium and coarse pumice lapilli occur in most ash intervals. A 7 cm thick layer of light-colored pumice lapilli with ash is interspersed within an ash interval at 17.42–17.49 mbsf.

Selected smear slides show representative lithologies of Subunit Ia. Microscopically, ash layers are characterized by colorless blocky to cuspate and pumiceous glass shards (Figure **F8A**). Vesicles are typically elongated to tubular and, in rare cases, round. Crystals of plagioclase and opaques, and rare pyroxene, are also present. Lithic fragments are typically volcanic or sedimentary. Tuffaceous

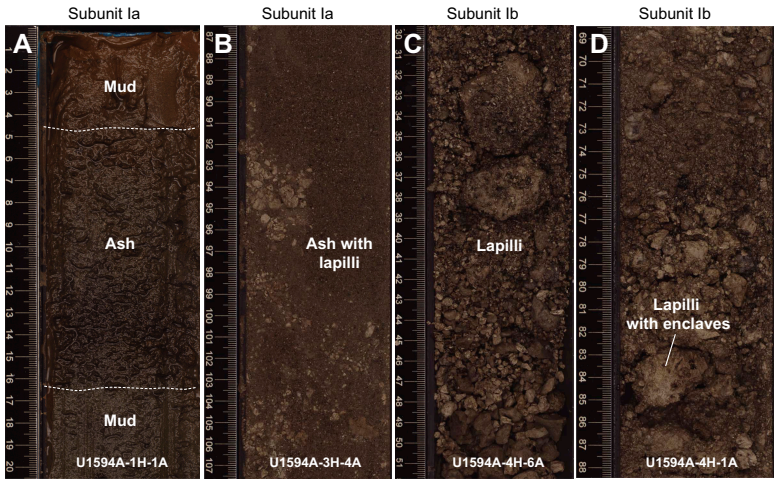

Figure F7. Common lithologies, Hole U1594A. Subunit Ia: (A) mud and intercalated ash and (B) ash with subrounded gray lapilli. Subunit Ib: (C) lapilli with gray pumice, mafic enclave, and banded pumice and (D) tan-colored pumice lapilli with some of the lapilli containing mafic enclaves.

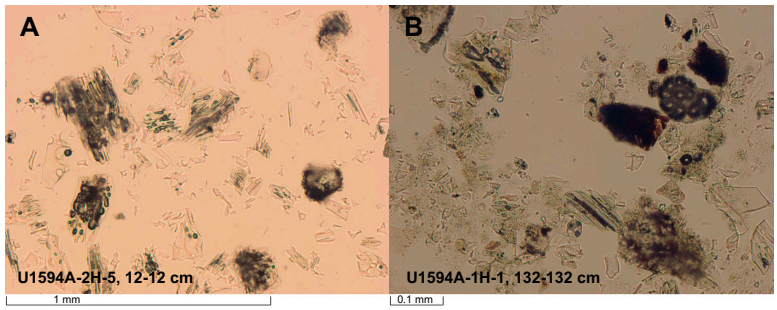

Figure F8. Representative lithologies from Subunit Ia, Hole U1594A. A. Volcanic ash characterized by transparent blocky, nonvesicular, and pumiceous glass shards. B. Tuffaceous mud showing blocks and vesicular glass shards, crystals, microfossils (e.g., foraminifera) and lithic clasts.

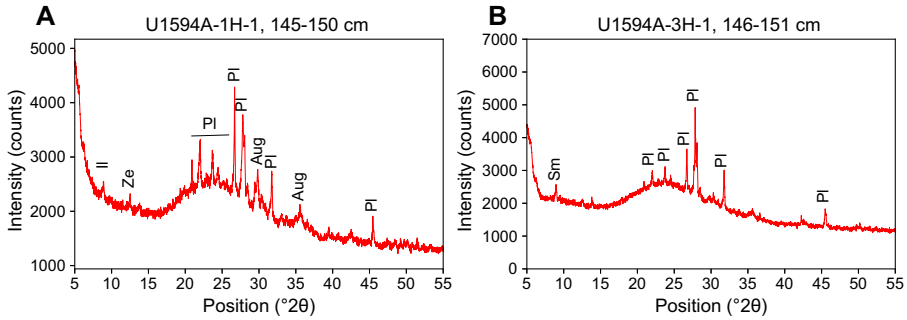

Figure F9. Selected XRD spectra of Subunit Ia volcanic lithologies (ash), Hole U1594A. A, B. Characteristic hump at low °2θ indicates the presence of volcanic glass. Identified crystalline phases are Ca-rich plagioclase, augite, clay minerals typical of the illite group and smectite group (montmorillonite), and zeolite. Il = illite, Ze = zeolite, Pl = Ca-rich plagioclase, Aug = augite, Sm = smectite.

mud is characterized by blocky to pumiceous transparent glass, crystals such as plagioclase and rare pyroxene, biogenic clasts (e.g., foraminifera, diatoms, and sponge spicules), calcareous nannofossils, and lithic clasts of sedimentary and volcanic rock (Figure **F8B**).

3.2.1.2. Subunit Ib

Subunit Ib extends from 20.74 to 50.09 mbsf in Hole U1594A (Figure **F3**). Because the bottom was not recovered, the total thickness of this subunit is >33.37 m. Subunit Ib is entirely volcanic lithologies, consisting of lapilli-ash and lapilli with lesser ash (Figure **F7C, F7D**). The top of Subunit Ib is recognized by a distinct change from ash-dominated lithologies in Subunit Ia to brown to grayish brown coarse lapilli–dominated lithologies of Subunit Ib. This subunit boundary is also marked by a distinct change in bulk density, *P*-wave velocities, MS, and NGR (see **Physical properties**). Bulk density decreases significantly at the subunit boundary, whereas the decrease in NGR across the boundary is more gradual. *P*-wave velocities and MS also display a sharp change at the subunit boundary, becoming strikingly more scattered but, on average, higher in Subunit Ib.

Lapilli-ash and lapilli intervals are grayish brown and consist of subrounded to subangular pumice lapilli. These are typically brownish or gray to dark gray, with lighter colored and black pumice clasts present in some intervals. They have a vesicular to highly vesicular texture, with vesicle shapes ranging from elongate to tubular. Banded pumices, characterized by dark-colored bands in light-colored or brown pumice, and small mafic enclaves are common in some intervals.

No smear slides were prepared for Subunit 1b.

3.3. X-ray diffraction

XRD data were collected from three IW squeeze cake sediment residues from Hole U1594A. The analyzed samples comprise volcanic lithologies (ash) from Lithostratigraphic Subunit Ia only. XRD spectra of two ash samples are shown in Figure **F9**. As reported in previous site chapters, the volcanic ash samples from Hole U1594A show a characteristic hump at low °2θ, indicating the presence of volcanic glass. The only identified crystalline phases in the ash samples are Ca-rich plagioclase, augite, clay minerals of the illite group or smectite group (montmorillonite), and zeolite.

4. Stratigraphic correlation

Because only one hole was drilled, no stratigraphic correlation could be made at Site U1594.

5. Structural geology

No structures with measurable orientations were identified at Site U1594. Although there were some bedding planes, core-induced disturbance prevented orientation measurements.

6. Biostratigraphy

Planktonic and benthic foraminifera and calcareous nannofossils were examined from core catcher samples from Hole U1594A to assess the paleoenvironmental conditions of Site U1594.

Site U1594 cored the sedimentary sequence in the southeast portion of the Santorini caldera and recovered a 51.7 m thick sequence composed primarily of volcanogenic sediments. Very rare planktonic and benthic foraminifera are found in core catcher samples in the form of *Globoturborotalita rubescens* in Sample 398-U1594A-1H-CC, 0–8 cm (Table **T3**; Figure **F10**), and *Sorites orbiculus* in Sample 4H-CC, 9–10 cm (Table **T4**), respectively. Additionally, very rare occurrences of the calcareous nannofossils *Emiliania huxleyi* and *Gephyrocapsa* spp. (small form) are found in Sample 3H-CC, 10–11 cm (Table **T5**; Figure **F11**). This assemblage indicates an age of younger than 0.265 Ma (Raffi et al., 2006).

Table T3. Distribution of planktonic foraminifera, Site U1594. **Download table in CSV format.**

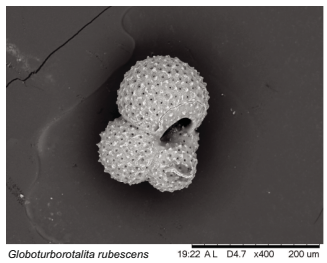

Figure F10. Planktonic foraminifera. *Globoturborotalita rubescens* (398-U1594A-1H-CC, 0–8 cm).

Table T4. Distribution of benthic foraminifera, Site U1594. **Download table in CSV format.**

Table T5. Distribution of calcareous nannofossils, Site U1594. **Download table in CSV format.**

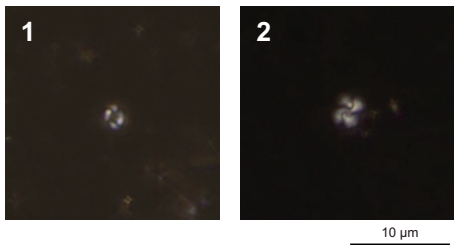

Figure F11. Calcareous nannofossils (398-U1594A-2H-CC, 17–19 cm). 1. *Emiliania huxleyi* (Lohmann) Hay and Mohler. 2. *Gephyrocapsa* spp. (small form).

7. Paleomagnetism

None of the cores recovered at this site were suitable for paleomagnetic analysis.

8. Physical properties

There is a general trend of increasing *P*-wave velocity and MS with increasing depth at Site U1594. More than 40% of discrete samples have grain densities <2.0 g/cm^3, and grain density decreases with increasing depth. Thermal conductivity is lower than typical values for sediments at similar depths.

8.1. Whole-round GRA density, MS, *P*-wave velocity, and NGR

Figure **F12** summarizes data collected on whole-round cores using the gamma ray attenuation (GRA) densitometer, MS loop, and *P*-wave logger on the Whole-Round Multisensor Logger (WRMSL) as well as NGR. All cited depths are on the CSF-A scale. There are some systematic sources of error in these data that should be considered when interpreting absolute values and trends.

- Redistribution of unconsolidated volcaniclastic materials in core liners during coring and on the core retrieving platform can lead to sorting by particle size and density and, hence, changes in physical properties.
- Core liners sometimes contained large amounts of water. Thus, whole-round measurements in sections that match discrete measured values on split cores are most reliable.

Overall, there is a general trend of increasing *P*-wave velocity and MS and decreasing NGR with increasing depth.

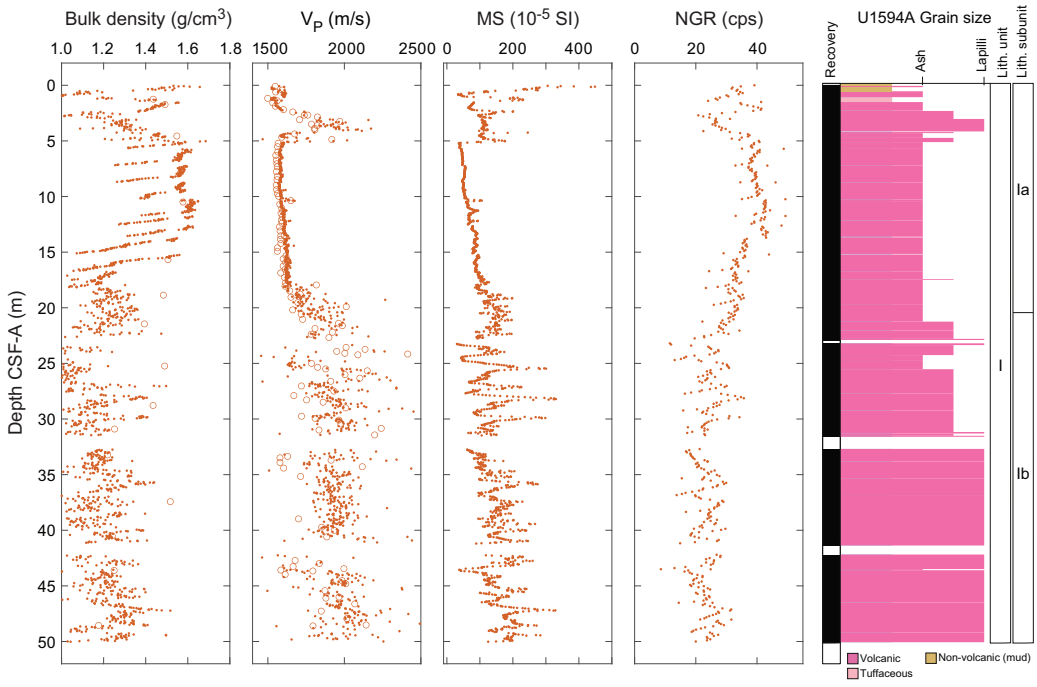

Figure F12. Physical properties, Site U1594. Dots = whole-round measurements, open symbols = discrete sample measurements. cps = counts per second.

8.2. Discrete measurements

8.2.1. Material strength

Sediment strength was measured with a pocket penetrometer (PP) on the catwalk immediately after section splitting. Automated vane shear (AVS) strength measurements were made on working-half sections. Because volcaniclastic materials are not suitable for these measurements, few measurements could be made (seven AVS and one PP) (Figure **F13**; Table **T6**).

8.2.2. *P*-wave velocity

A total of 130 *P*-wave velocity measurements were conducted on working-half sections (Figure **F13**; Table **T7**). Discrete measurements of *P*-wave velocity on working-half core sections are similar to those measured using the WRMSL on whole-round cores (Figure **F12**). A high *P*-wave velocity layer is located between 3 and 5 mbsf. *P*-wave velocity also increases with depth downhole. The large scatter below 20 mbsf arises from a combination of measurements that capture bulk sediment properties (lower values) and measurements made across a small number of lapilli clasts (larger values). For lapilli and larger sized clasts, the particle size was a substantial fraction of the distance between the two calipers used to make the measurements; hence, the measurements may not be representative of true bulk properties (i.e., sample size is not much larger than a representative elementary volume).

8.2.3. Moisture and density

A total of 17 discrete samples were collected for MAD measurements (Figure **F13**; Table **T8**). Bulk density derived by MAD measurements on discrete samples should be more reliable than GRA data from WRMSL measurements on whole-round cores, although in both cases coring and recovery disturbances may have impacted measured values.

Porosity ranges 51–80 vol% (mean = 66 vol%; standard deviation = 8 vol%). Bulk density ranges 1.2–1.6 g/cm^3 (mean = 1.41 g/cm^3). Bulk density does not obviously increase with depth.

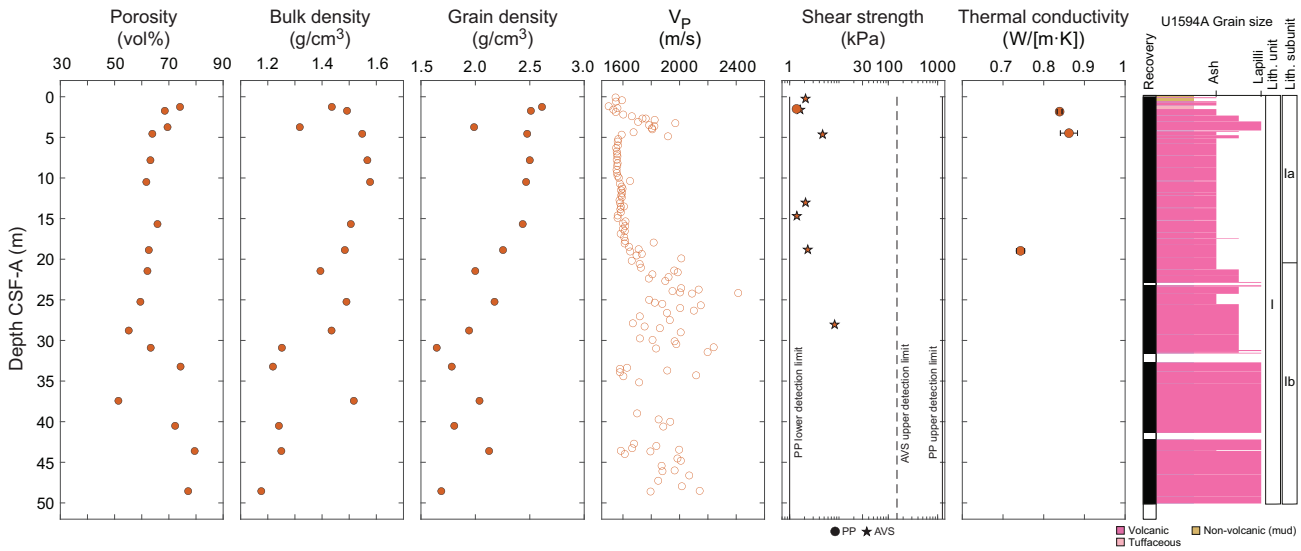

Figure F13. Discrete physical properties measurements, Hole U1594A.

Table T6. Shear strength, Site U1594. **Download table in CSV format.**

Table T7. *P*-wave velocity, Site U1594. **Download table in CSV format.**

Table T8. MAD measurements, Site U1594. **Download table in CSV format.**

Table T9. Thermal conductivity, Site U1594. **Download table in CSV format.**

Grain density ranges 1.6–2.6 g/cm^3 (mean = 2.1 g/cm^3; median = 2.1 g/cm^3). A total of 41% of discrete samples have grain densities <2.0 g/cm^3, and grain density decreases with increasing depth.

8.2.4. Thermal conductivity

A total of three thermal conductivity measurements were made on selected working-half sections (Table **T9**). Measurements could not be made on coarse, volcaniclastic materials; hence, the values we report are not representative of the full range of recovered lithologies. There is no apparent increase in thermal conductivity with increasing depth (Figure **F13**). Compared to typical sediments, in which thermal conductivity is close to 1 W/(m·K) at these depths below seafloor, thermal conductivity is low in volcaniclastic sediments at Site U1594.

9. Geochemistry

9.1. Volcaniclastic bulk geochemistry

To determine the geochemistry of the volcanic and tuffaceous materials, four tephra and ash samples were handpicked from various layers in Hole U1594A. Following cleaning, grinding, fusion, and dissolution, the materials were analyzed shipboard for major (Si, Al, Fe, Mg, and Ca), minor (Ti, Mn, Na, K, and P), and trace (Sc, V, Cr, Co, Ni, Cu, Zn, Rb, Sr, Y, Zr, Nb, Ba, Ce, and Nd) elements using inductively coupled plasma–atomic emission spectroscopy (ICP-AES) (see **Geochemistry** in the Expedition 398 methods chapter [Kutterolf et al., 2024] for analytical technique). Several unknown samples were run multiple times to determine analytical reproducibility.

9.1.1. ICP-AES: major, minor, and trace elements

All the volcaniclastic units sampled were classified as dacites or trachydacites (Table **T10**; Figure **F14**). Bulk chemistry values are less evolved than glass chemistry reported in Kutterolf et al. (2021), as expected, due to bulk analyses including both minerals and glass.

Concentrations are reported for all analyzed trace elements, but Ce, Cr, Cu, Nb, Ni, P, Rb, S, and V were below detection limits in the majority of samples and are not shown for respective samples in Table **T10**; volcaniclastic analytical errors are ±1% for major elements and ±5%–10% for trace elements (see **Geochemistry** in the Expedition 398 methods chapter [Kutterolf et al., 2024]). Trace element ratios were used to broadly discriminate between the volcanic centers of Kolumbo, Santorini, and Christiana.

9.2. Interstitial water geochemistry

To determine the inorganic constituents of IW, a total of four water samples were taken from the mudline and whole-round squeezing of sediment intervals at Site U1594. Aliquots of IW were used for shipboard analyses, and the remaining water was retained for shore-based analysis, following protocols specified by individual scientists. One sample (398-U1594A-1H-1) did not have enough water to analyze for alkalinity or pH. The retrieved pore waters were analyzed shipboard for salinity, alkalinity, pH, major anions (Cl^-, SO_4^{2-}, and Br^-), major cations (Ca^{2+}, Na^+, Mg^{2+}, and K^+), and major (S, Ca, Mg, K, and Na) and minor (B, Ba, Fe, Li, Mn, P, Si, and Sr) elements using the methods described in **Geochemistry** in the Expedition 398 methods chapter (Kutterolf et al., 2024).

9.2.1. Salinity, alkalinity, and pH

Salinity values are 40 throughout the hole (Table **T11**; Figure **F15**). No variations were recorded.

Alkalinity increases slightly from the mudline (2.6 mM) to 12.6 mbsf (5.7 mM) in Hole U1594A, followed by a slight decrease with depth to the base of the hole at 15.16 mbsf (Table **T11**; Figure **F15**).

Values for pH show slight variation within the sampled depths, ranging 7.8–7.9 (Table **T11**; Figure **F15**).

9.2.2. Bromide, chloride, boron, sodium, potassium, magnesium, calcium, and sulfate

There are small variations in B and major cations and anions except Br^-, which remains constant with depth (Table **T12**; Figure **F16**). Calcium, Mg^{2+}, Na^+, Cl^-, and B all increase slightly from the mudline to 15.2 mbsf. Potassium decreases from 11.7 mM in the uppermost IW sample at 1.44

Table T10. ICP-AES data for major, minor, and trace elements, Site U1594. **Download table in CSV format.**

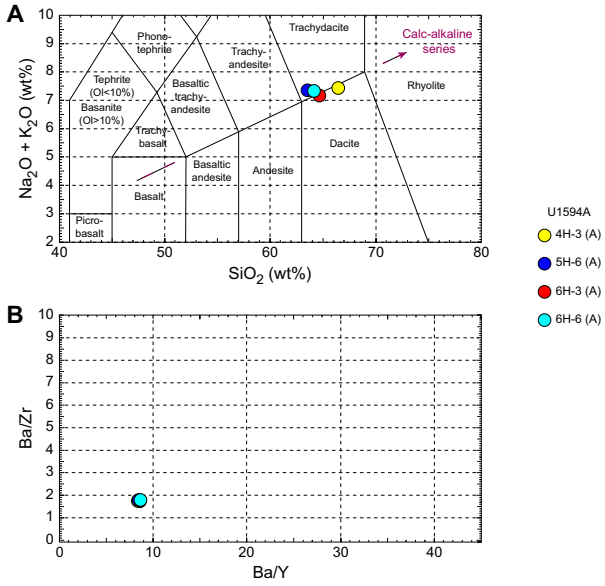

Figure F14. ICP-AES analyses of selected volcaniclastic units used to discriminate between potential volcanic sources, Hole U1594A. A. Total alkali vs. SiO_2 plot with the rock nomenclature of Le Maitre et al. (2002) overlain used for sample naming. Ol = olivine. B. Ba/Y vs. Ba/Zr plot used to correlate samples.

Table T11. Alkalinity, pH, and salinity values, Site U1594. **Download table in CSV format.**

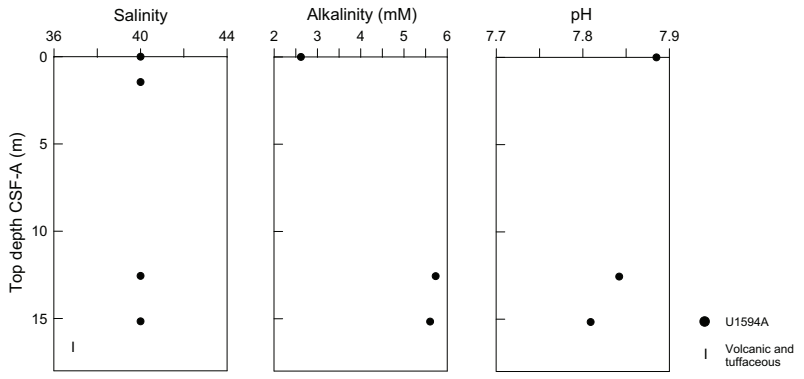

Figure F15. IW salinity, alkalinity, and pH, Site U1594. Lithostratigraphic Unit I is described in Lithostratigraphy.

Table T12. IW data for major anions and cations measured using ion chromatography and major and minor elements measured using ICP-AES, Site U1594. **Download table in CSV format.**

mbsf to 8.6 mM at 15.2 mbsf. Sulfate values are relatively constant with depth, although they are slightly lower at 1.4 and 12.6 mbsf.

9.2.3. Lithium, strontium, iron, manganese, phosphorus, barium, and silicon

There are larger variations in Li, Sr, Mn, Ba, and Si than for cations and anions (Table **T12**; Figure **F17**). Lithium increases from 30.4 to 48.4 µM from 1.4 to 15.2 mbsf. Strontium and Si peak at 12.6 mbsf. The highest values of Ba, Fe, Mn, and P occur at 1.4 mbsf. Iron and P are below detection limit in all other samples and thus are not plotted, but their values are 164.6 and 8.2 µM, respectively, at this depth.

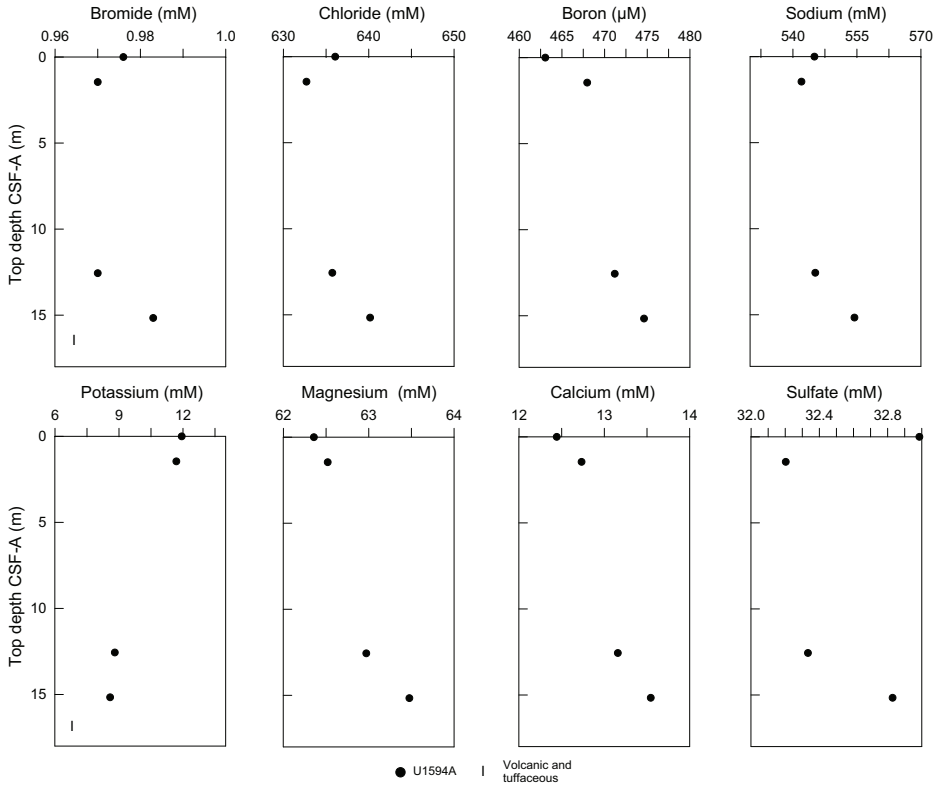

Figure F16. IC and ICP-AES concentrations of Br, Cl, B, Na, K, Mg, Ca, and SO_4^{2-} in IW samples, Site U1594. Lithostratigraphic Unit I is described in Lithostratigraphy.

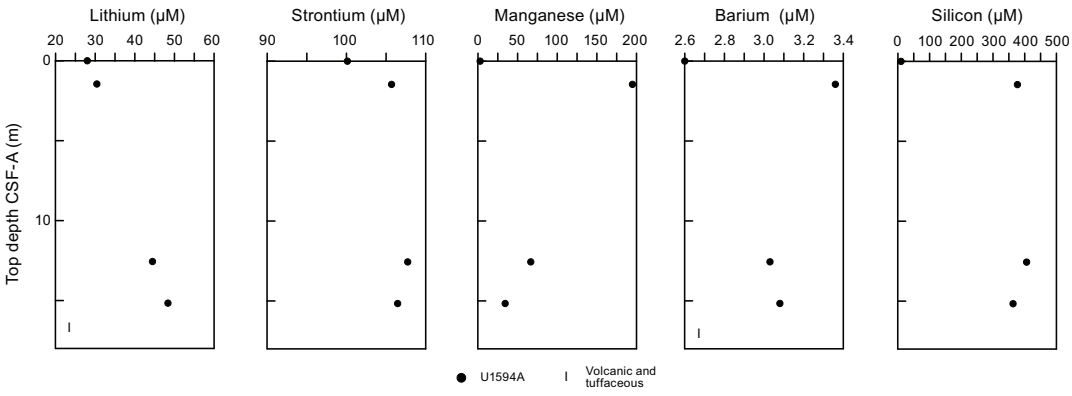

Figure F17. ICP-AES concentrations of Li, Sr, Mn, Ba, and Si in IW samples, Site U1594. Lithostratigraphic Unit I is described in Lithostratigraphy.

Table T13. Total inorganic carbon (TIC), percent $CaCO_3$, TC, total nitrogen (TN), and TOC data, Site U1594. **Download table in CSV format.**

Table T14. Microbiology samples, Site U1594. **Download table in CSV format.**

9.3. Sediment bulk geochemistry

Three sediment samples were analyzed for bulk geochemistry (Table **T13**). All were analyzed for total carbon, hydrogen, and nitrogen (CHN) and for inorganic carbon and carbonate content (see **Geochemistry** in the Expedition 398 methods chapter [Kutterolf et al., 2024]). For CHN analysis, duplicates were run for ~10% of the samples to determine analytical reproducibility (standard deviation: N = 0.01; C = 0.04). Carbonate values peaked at 2.25 wt% (Table **T13**).

9.3.1. Sapropel identification

Total organic carbon (TOC) was calculated using total carbon and inorganic carbon values. Following the convention set forth by Kidd et al. (1978), units with TOC values >2.0 wt% were identified as sapropels and units with TOC values of 0.5–2.0 wt% were identified as sapropelitic. Using these values, no units were identified as sapropels or sapropelitic (Table **T13**).

9.4. Headspace gas analysis

Headspace gas analyses were performed at a resolution of one sample per full-length core (9.5 m advance) throughout Hole U1594A. The aim was to monitor the presence and abundance of C_1–C_3 hydrocarbons as part of the standard International Ocean Discovery Program safety protocol (Pimmel and Claypool, 2001). A total of six headspace gas samples from this hole were analyzed using gas chromatography (see **Geochemistry** in the Expedition 398 methods chapter [Kutterolf et al., 2024]). Methane, ethane, and propane concentrations were below the detection limit through all of Hole U1594A.

10. Microbiology

For Site U1594, six whole-round core samples were collected for microbial community composition analysis (Table **T14**).

References

Druitt, T., Kutterolf, S., and Höfig, T.W., 2022. Expedition 398 Scientific Prospectus: Hellenic Arc Volcanic Field. International Ocean Discovery Program. **https://doi.org/10.14379/iodp.sp.398.2022**

Druitt, T.H., Kutterolf, S., Ronge, T.A., Beethe, S., Bernard, A., Berthod, C., Chen, H., Chiyonobu, S., Clark, A., DeBari, S., Fernandez Perez, T.I., Gertisser, R., Hübscher, C., Johnston, R.M., Jones, C., Joshi, K.B., Kletetschka, G., Koukousioura, O., Li, X., Manga, M., McCanta, M., McIntosh, I., Morris, A., Nomikou, P., Pank, K., Peccia, A., Polymenakou, P.N., Preine, J., Tominaga, M., Woodhouse, A., and Yamamoto, Y., 2024. Site U1589. In Druitt, T.H., Kutterolf, S., Ronge, T.A., and the Expedition 398 Scientists, Hellenic Arc Volcanic Field. Proceedings of the International Ocean Discovery Program, 398: College Station, TX (International Ocean Discovery Program). **https://doi.org/10.14379/iodp.proc.398.103.2024**

Fisher, R.V., and Schmincke, H.-U., 1984. Pyroclastic Rocks: Berlin (Springer). **https://doi.org/10.1007/978-3-642-74864-6**

Johnston, E.N., Sparks, R.S.J., Nomikou, P., Livanos, I., Carey, S., Phillips, J.C., and Sigurdsson, H., 2015. Stratigraphic relations of Santorini's intracaldera fill and implications for the rate of post-caldera volcanism. Journal of the Geological Society (London, UK), 172(3):323–335. **https://doi.org/10.1144/jgs2013-114**

Jutzeler, M., White, J.D.L., Talling, P.J., McCanta, M., Morgan, S., Le Friant, A., and Ishizuka, O., 2014. Coring disturbances in IODP piston cores with implications for offshore record of volcanic events and the Missoula megafloods. Geochemistry, Geophysics, Geosystems, 15(9):3572–3590. **https://doi.org/10.1002/2014GC005447**

Kidd, R.B., Cita, M.B., and Ryan, W.B.F., 1978. Stratigraphy of eastern Mediterranean sapropel sequences recovered during DSDP Leg 42A and their paleoenvironmental significance. In Hsü, K., Montadert, L., et al., Initial Reports of the Deep Sea Drilling Project. 42(1): Washington, DC (US Government Printing Office), 421–443. **https://doi.org/10.2973/dsdp.proc.42-1.113-1.1978**

Kutterolf, S., Druitt, T.H., Ronge, T.A., Beethe, S., Bernard, A., Berthod, C., Chen, H., Chiyonobu, S., Clark, A., DeBari, S., Fernandez Perez, T.I., Gertisser, R., Hübscher, C., Johnston, R.M., Jones, C., Joshi, K.B., Kletetschka, G., Koukousioura, O., Li, X., Manga, M., McCanta, M., McIntosh, I., Morris, A., Nomikou, P., Pank, K., Peccia, A., Polymenakou, P.N., Preine, J., Tominaga, M., Woodhouse, A., and Yamamoto, Y., 2024. Expedition 398 methods. In Druitt, T.H., Kutterolf, S., Ronge, T.A., and the Expedition 398 Scientists, Hellenic Arc Volcanic Field. Proceedings of the International Ocean Discovery Program, 398: College Station, TX (International Ocean Discovery Program). **https://doi.org/10.14379/iodp.proc.398.102.2024**

Kutterolf, S., Freundt, A., Hansteen, T.H., Dettbarn, R., Hampel, F., Sievers, C., Wittig, C., Allen, S.R., Druitt, T.H., McPhie, J., Nomikou, P., Pank, K., Schindlbeck-Belo, J.C., Wang, K.-L., Lee, H.-Y., and Friedrichs, B., 2021. The medial offshore record of explosive volcanism along the central to eastern Aegean Volcanic Arc: 1. tephrostratigraphic correlations. Geochemistry, Geophysics, Geosystems, 22(12):e2021GC010010. **https://doi.org/10.1029/2021GC010010**

Le Maitre, R.W., Steckeisen, A., Zanettin, B., Le Bas, M.J., Bonin, B., and Bateman, P. (Eds.), 2002. Igneous Rocks: A Classification and Glossary of Terms (Second edition): Cambridge, UK (Cambridge University Press). **https://doi.org/10.1017/CBO9780511535581**

Nomikou, P., Druitt, T.H., Hübscher, C., Mather, T.A., Paulatto, M., Kalnins, L.M., Kelfoun, K., Papanikolaou, D., Bejelou, K., Lampridou, D., Pyle, D.M., Carey, S., Watts, A.B., Weiß, B., and Parks, M.M., 2016. Post-eruptive flooding of Santorini caldera and implications for tsunami generation. Nature Communications, 7(1):13332. **https://doi.org/10.1038/ncomms13332**

Pimmel, A., and Claypool, G., 2001. Introduction to shipboard organic geochemistry on the JOIDES Resolution. Ocean Drilling Program Technical Note, 30. **https://doi.org/10.2973/odp.tn.30.2001**

Raffi, I., Backman, J., Fornaciari, E., Pälike, H., Rio, D., Lourens, L., and Hilgen, F., 2006. A review of calcareous nannofossil astrobiochronology encompassing the past 25 million years. Quaternary Science Reviews, 25(23):3113–3137. **https://doi.org/10.1016/j.quascirev.2006.07.007**